Imaging of sharp lateral variations in the subsoil: a numerical comparison of surface-wave based methods

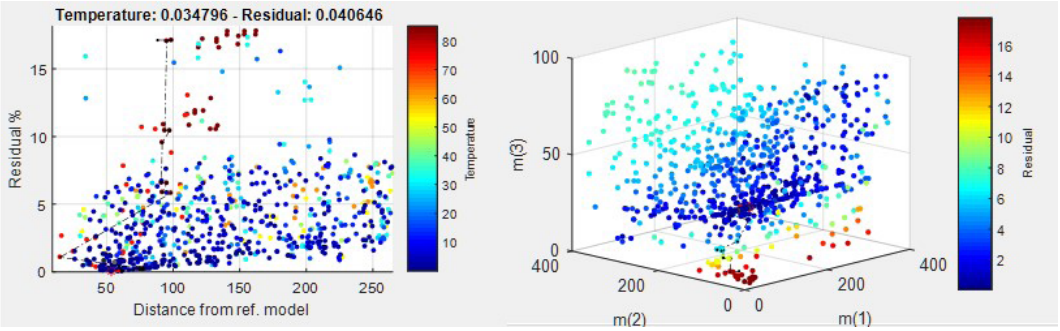

Fig. 3 - Simulated Annealing inversion evolution.

of the inverted values, as standard deviation of the posterior model normalized to the standard deviation of the prior model (Fig. 2 right). We tested many hybrid inversion sequences on the tutorial model: a very interesting approach is a first phase of SA, in order to place the current candidate point in the region of the global minimum, followed by a BLI, that pushes in few steps the candidate to the global solution.

In conclusion, complex inverse problems can be tackled with hybrid procedures, involving global and Bayesian methods. The whole process has to be preferably supervised. In this framework, the analysis tools presented here are very effective in highlighting "in real time" the most important information about the inversion status, the sensitivity of the observed data with respect to the model parameters, and the accuracy of the solution.

References

Bosisio, A., Drufuca, G., Rovetta, D.; The concept of distance in global optimization applied to non-linear inverse problems, Inverse problems in science & engineering, 22, 683-706, 2014.

Constable S.; Ten years of marine CSEM for hydrocarbon exploration. Geophysics, 75, A67–75A81, 2010.

Constable, S., and C. J. Weiss, Mapping thin resistors and hydrocarbons with marine EM methods: Insights from 1D modeling: Geophysics, 71, 2, G43–G51, 2006.

Corana, A., Marchesi, M., Martini, C., Ridella, S.; Minimizing Multimodal Functions of Continuous Variables with the

Simulated Annealing Algorithm; ACM Transactions on Mathematical Software, 13,262-280, 1987.

Hastings,W.K., *Monte Carlo sampling methods using Markov chains and their applications*, Biometrikam, 57, 97-109, 1970

Kirkpatrick, S., Gelatt, C.D., Vecchi, M.P.; Optimization by Simulated Annealing, Science, 1983.

Metropolis N., Rosenbluth A.W., Rosenbluth M.N., Teller A.H., and Teller E., Equation of State Calculations by Fast Computing Machines, J.Chem.Phys., 1, 1087-1092, 1953.

Vandone, V., Chiappa, F., Bernasconi G., Csem Sharp and Stable Imaging by Means of Probabilistic Inversion, Contractions-By-Bisections Line Search and Full Covariance Operator, Atti GNGTS, 2014.

IMAGING OF SHARP LATERAL VARIATIONS IN THE SUBSOIL: A NUMERICAL COMPARISON OF SURFACE-WAVE BASED METHODS

C. Colombero[1], E.I. Cojocariu[2], C. Comina[1], L.V. Socco[2]

[1] *Dipartimento di Scienze della Terra, Università degli Studi di Torino, Italy*

[2] *Dipartimento di Ingegneria dell'Ambiente, del Territorio e delle Infrastrutture, Politecnico di Torino, Italy*

Introduction. Near-surface heterogeneities including fractures, faults, cavities, buried low-velocity bodies or slopes with strong lateral contrasts in physical and mechanical properties, are a common target of investigation in surface seismic surveys. Dealing with such abrupt,

localized and marked lateral variations, P- and S-wave tomographic interpretations may results inadequate to effectively delineate location and depth of these sharp anomalies with reliable detail. Since surface waves (SWs) propagate parallel to the ground surface, their analysis can be used as an additional tool for the detection of these lateral heterogeneities. Several SW based methods have been developed to locate the sharp lateral variation and to estimate its embedment depth. For location purposes, the energy computation on the recorded seismograms can be a useful tool to highlight energy concentrations due to back-reflection of energy at the lateral variation or to energy trapping within the discontinuity (Nasseri-Moghaddam *et al*., 2005; Bergamo and Socco, 2014; Colombero *et al*., 2017). Analogously, the computation of the energy decay exponent (γ) can provide a global estimation of the discontinuity location. In particular, disregarding the effect of intrinsic attenuation and compensating the recorded traces for SW geometrical spreading, γ is expected to be zero in a homogeneous medium, and thus strong deviations from this value can be interpreted as the effect of either energy concentrations ($\gamma<0$) or energy decays ($\gamma>0$) induced by reflections caused by the lateral variation. To additionally retrieve a depth estimation, techniques based on the evaluation of the attenuation coefficient (α), describing the trend of energy decay as a function of frequency, can be adopted. The value of α is indeed related to the mechanical properties of the subsoil affected by the propagation in different frequency components of Rayleigh waves. When sharp heterogeneities are present in the subsoil the value of α is strongly influenced by the reflection of energy at the interfaces, and hence, abrupt variations can be interpreted as the effect of lateral discontinuities in the subsurface. Since the depth of penetration of Rayleigh waves increases as their frequency decreases, only low frequencies of the incident wave are expected to have enough energy below the discontinuity to be transmitted. Particularly, identifying the threshold between higher frequencies that undergo backward reflection or are trapped within the discontinuity and undisturbed lower frequencies can provide the embedment depth of the discontinuity. Generally, this depth could be roughly estimated as 1/3 of the wavelength, and thus the ratio between the mean Rayleigh-wave velocity (V_R) and three times the identified cut-off frequency. Both γ and α methods were originally designed for single-fold data, and later extended to multifold data by Bergamo and Socco (2014), to improve the reliability and interpretation of the results. In the same work, single-fold autospectrum plots (Zerwer *et al*., 2005), displaying the energy content of seismogram as a function of offset and frequency, were compared to the previous methods for the simultaneous achievement of both discontinuity location and depth estimation purposes. Finally, when the location is known, the Transmitted-over-Incident (T/I) spectral ratio technique (Hévin *et al*., 1998; Bièvre *et al*., 2012; Colombero *et al*., 2017) can help to further constrain the discontinuity depth. From the ratio between the Fourier spectra of transmitted traces (after the discontinuity) and incident traces (before the discontinuity), the cut-off frequency can be determined as well. In this work, these five SW based procedures (energy, γ, α, autospectrum and T/I spectral ratio methods) are simultaneously applied to a synthetic dataset, for a cross-comparison of the results in terms of both location and depth estimation of a shallow discontinuity. Novel attempts to reach a single subsurface imaging from the processing of multifold data are presented.

Methods. A 2D finite-element-model was built in Comsol Multiphysics to retrieve a set of synthetic seismograms for testing the different SW based methods. Large model dimensions were chosen to simulate a half-space configuration (Fig. 1a). To avoid strong wave reflections at the borders of the model, low-reflecting boundaries were applied at the bottom and lateral sides of the domain and the bottom corner points were fixed to zero displacement. The upper surface was left free; in its central part a synthetic array of 72 geophones with 0.5-m spacing was simulated. A rectangular heterogeneity (7-m wide and 2-m deep) was built in the center of the array, between geophones G29-G30 and G43-G44 (Fig. 1b). A marked contrast in physical and mechanical properties between the material inside and outside the box was assigned, as summarized in Tab. 1. For both materials, Rayleigh damping was introduced in the model.

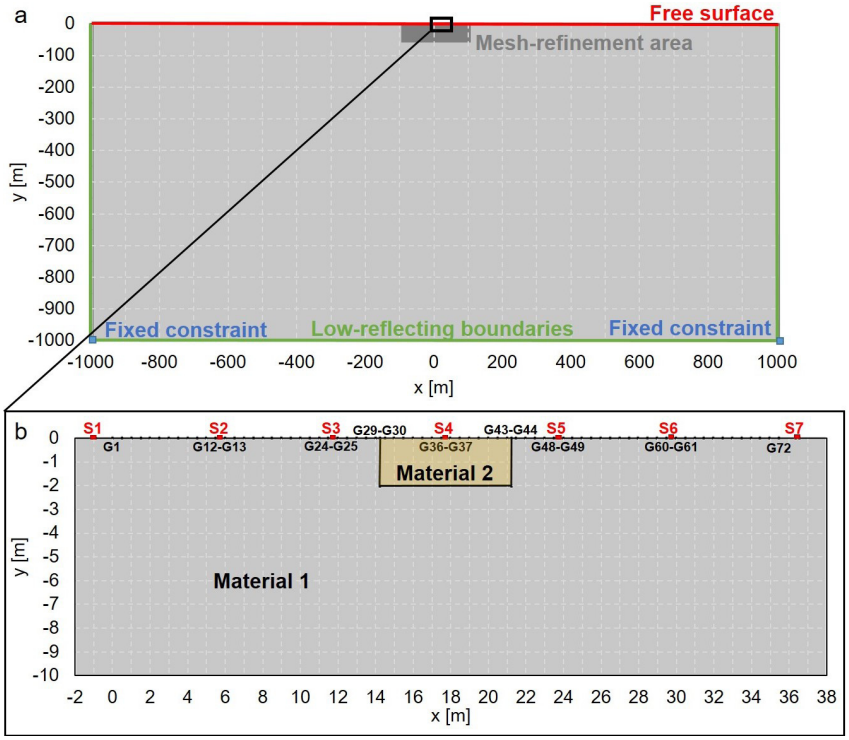

Fig. 1 - a) 2D finite-element model used for the generation of the synthetic seismograms. b) Zoom on the upper central part of the model (black rectangle, in a) with the synthetic array configuration, source locations and discontinuity geometry.

Free triangular mesh was built for the whole model, a mesh refinement window of 200x50 m was applied around and below the synthetic array in order to respect a maximum element size suitable for the propagating wavelengths in both materials.

Tab. 1 - Physical and mechanical parameters adopted in the simulations for materials outside (1) and inside (2) the subsurface heterogeneity.

	ρ [kg/m^3]	E [MPa]	ν [-]	V_P [m/s]	V_S [m/s]	V_R [m/s]	Q_{factor} [-]
Material 1	2200	180	0.3	330	175	162	20
Material 2	1900	90	0.3	200	110	102	15

A Ricker wavelet centered at 50 Hz was chosen as seismic input for the model, in seven source positions, located at the ends and within the array, with a step of 12 geophones (S1-S7, in Fig. 1b). Synthetic seismograms were generated for each source location. After recovering geometrical spreading in the seismograms, the total energy of each trace was calculated as the sum of the squared spectral amplitudes in the 5-75 Hz band and then normalized to the maximum of each seismogram. The energy decay exponent was calculated as the local slope of the energy-distance plot in a bilogarithmic scale, shifting a moving window along the seismic line. For each window position, calculated γ were averaged from all the available shots, distinguishing between positive and negative offsets. The standard deviation on each window was retrieved as well to consider estimation uncertainties. Using the same moving windows along the energy-distance plot, the attenuation coefficient of each frequency component was obtained as the local slope of the energy$_f$-distance plot in a double natural logarithmic scale. For each window

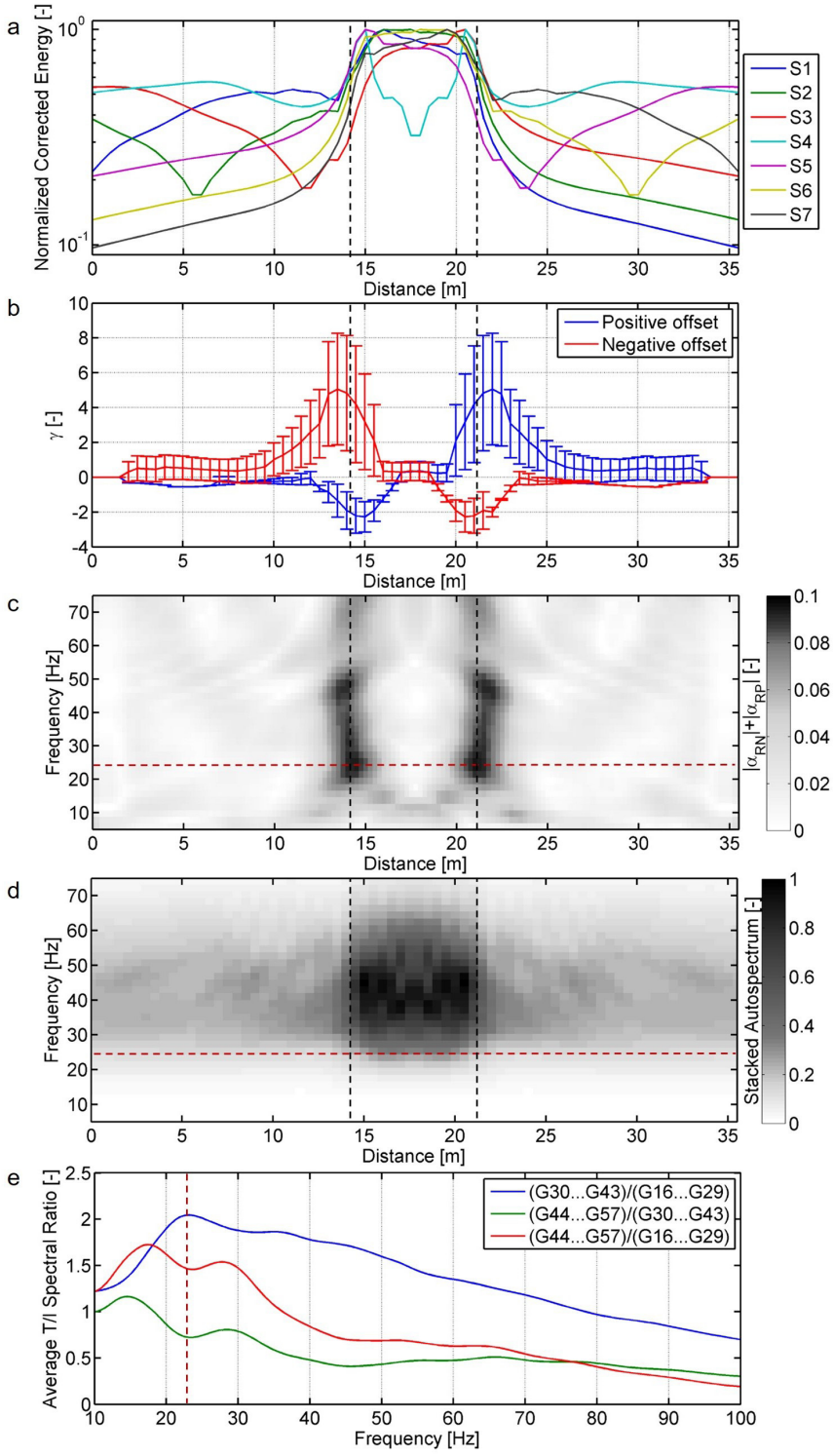

Fig. 2 - Results of SW based methods: a) normalized energy; b) energy decay exponent; c) stacking of positive- and negative-offset attenuation coefficient absolute variation; d) stacking of autospectrum plots of all source locations; e) average T/I spectral ratios.

position, obtained values were averaged and normalized to the related standard deviation (α_{RP} and α_{RN} for positive and negative offsets respectively). This normalization enabled to compare attenuation coefficients obtained for different frequencies and to identify abrupt variations. To obtain a single imaging for both positive and negative offsets, the absolute values of α_{RP} and α_{RN} were stacked in a single plot, in which maximum values are expected to highlight the strongest contrasts. The autospectral density of each seismogram was computed as the sum of the squared real and imaginary parts of each-trace Fourier Spectrum, after recovering geometrical spreading on the seismograms. The resulting autospectrum plots of all the shots were then stacked together to reduce the influence of the source location and highlight the effects of the heterogeneity. T/I spectral ratios were computed considering all the possible pairs between 14 geophones placed after and before the sharp lateral variations (for a total of 196 combinations) in three different T/I locations: inside/outside$_{left}$ the box [(G30…G43)/(G16…G29)], outside$_{right}$/inside the box [(G44…G57)/(G30…G43)], outside$_{right}$/outside$_{left}$ the box [(G44…G57)/(G16…G29)].

Results. The results of the five tested SW based methods are summarized in Fig. 2. Given the model geometry and mechanical properties, abrupt variations are expected at the box edges, at distances of approximately 14.25 m and 21.25 m. Dealing with depth estimation, considering an average V_R of 150 m/s in the first 10-m of the model and a known depth of 2 m for the box, a cut-off frequency around 23 Hz [$f=V_R/(3z)$] is expected. Theoretical location and cut-off frequency are highlighted in Fig. 2 with back and red dashed lines respectively. All the normalized energy curves (Fig. 2a) show high energy concentration within the box. Particularly, the shot located on the anomaly (S4) highlights sharp narrow energy concentrations at the box edges. Around these locations, the energy decay exponent (Fig. 2b) has marked variations from zero, both for positive and negative offsets. In particular, the real box edges are located between the minimum and maximum of the opposite offset curves. A clear discontinuity location is also obtained from the stacked plot of attenuation coefficient variations (Fig. 2c) and autospectra (Fig. 2d). A clear frequency cut-off is also found in Fig. 2c and Fig. 2d, approximately around the theoretical one. The average T/I spectral ratios (Fig. 2e) confirm the same frequency cut-off, with a local minimum for the T/I ratios related to traces located either across the right box edge or after and before the box. Conversely, while computing the T/I spectral ratios of traces located across the left box edge, given the energy concentration and the high-frequency trapping within the heterogeneity (thus more marked in the transmitted waveforms) a maximum is found at the same cut-off frequency.

Conclusions. Several SW based techniques for location and depth estimation of subsurface sharp lateral heterogeneities are available in literature. Since all these techniques were originally developed for single-fold configurations, the final data interpretation often resulted unclear and strongly dependent on the a-priori knowledge of the discontinuity location. Adapting these procedure to multifold data and improving the multi-fold already-existing techniques, towards a single imaging of the subsurface investigated by the array, has the advantage to strengthen the effects due to the discontinuity presence and to consequently improve reliability and interpretation of the results. In the present work, this was demonstrated on a simple synthetic study, but ongoing tests suggest the validity of the presented approach on real case studies, for both rock (i.e. detection and depth estimation of the open joints in a fractured rock mass) and soil mechanics issues (i.e. detection of loose formations in the overburden). Further synthetic tests will help to better constrain the sensitivity and uncertainties of each method to varying heterogeneity depths and to buried sharp lateral variations, not intersecting the free ground surface.

References

Bergamo P. and Socco L.V.; 2014: *Detection of sharp later discontinuities through the analysis of surface-wave propagation*. Geophysics, **79** (4), EN77-EN90.

Bièvre G., Jongmans D., Winiarski T. and Zumbo V.; 2012: *Application of geophysical measurements for assessing the role of fissures in water infiltration within a clay landslide (Trieves area, French Alps)*. Hydrol. Process, **26**, 2128-2142.

Colombero C., Baillet L., Comina C., Jongmans D. and Vinciguerra S.; 2017: *Characterization of the 3-D fracture setting of an unstable rock mass: From surface and seismic investigations to numerical modeling*. JGR: Solid Earth, **122**, 1-21. doi: 10.1002/2017jb014111

Hévin G., Abraham O., Pedersen H.A. and Campillo M.; 1998: *Characterisation of surface cracks with Rayleigh waves: a numerical model*. NDT&E International, **31**(4), 289-297.

Nasseri-Moghaddam A., Cascante G. and Hutchinson J.; 2005: *A New Quantitative Procedure to Determine the Location and Embedment Depth of a Void Using Surface Waves*. Journal of Environmental and Engineering Geophysics, **10**, 51-64.

Zerwer A., Polak M.A. and Santamarina J.C.; 2005: *Detection of surface breaking cracks in concrete members using Rayleigh waves*. Journal of Environmental and Engineering Geophysics, **10**, 295-306.

RPM ANALYSIS AND ADVANCED JOINT PROCESSING OF A SED (SWISS SEISMOLOGICAL SERVICE) DATASET

G. Dal Moro[1], L. Keller[2]

[1] *Institute of Rock Structure and Mechanics, Prague, Czech Republic*

[2] *roXplore, Amlikon-Bissegg, Switzerland*

In the framework of a series of site characterizations at some of the seismic monitoring stations operated by the Swiss Seismological Service (Schweizerischer ErdbebenDienst - SED), we recently tested an innovative method for the Holistic acquisition and analysis of the Surface waves (HS) recorded by means of a single 3-component (3C) geophone (Fig. 1).

The method originally consisted in the joint analysis of the group-velocity spectra of both the vertical (Z) and radial (R) component, together with the RVSR (Radial-to-Vertical Spectral Ratio) (Dal Moro *et al*., 2014, 2015).

We here introduce a further *object* aimed at both further constraining the inversion process (thus obtaining a even more robust shear-wave velocity profile), and at providing to the structural engineers quantitative information regarding the occurrence of Rayleigh-wave prograde motion, recently identified as potential critical factor for the stability of a structure in case of earthquake (Trifunac, 2009).

An effective way to analyze the actual Rayleigh-wave Particle Motion (RPM), was introduced in Dal Moro *et al*. (2017) through the computation, frequency by frequency, of the correlation coefficient between the radial component and the Hilbert transform of the vertical component of Rayleigh waves. The obtained RPM frequency curve (or frequency-offset surface in case of multi-offset data) provides quantitative information about the actual Rayleigh-wave motion (the RPM curve equals to +1 in case of perfectly retrograde motion and to -1 in case of prograde motion) and can be used to further constraining a joint inversion procedure (Dal Moro, 2017; Dal Moro and Puzzilli, 2017).

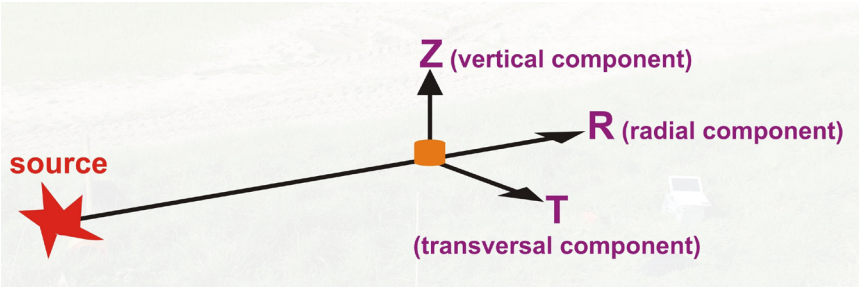

Fig. 1 - Multi-component (single-offset) acquisition of the active data used to implement the HS approach adopted for the present work.